Wear 522 (2023) 204685

Contents lists available at ScienceDirect

Wear

journal homepage: www.elsevier.com/locate/wear

Wear induced changes in surface topography during running-in of rolling-sliding contacts

Maruti Sai Dhiraj Sakhamuri [a,*], Terry J Harvey [a], Bernd Vierneusel [b], Robert J K Wood [a]

[a] nCATS, Dept of Mechanical Engineering, Faculty of Engineering and Physical Sciences, University of Southampton, Highfield, Southampton, UK
[b] Schaeffler Technologies AG & Co. KG, Georg-Schäfer-Straße 30, 97421, Schweinfurt, Germany

ARTICLE INFO

Handling Editor: Dr. M Dienwiebel

Keywords:
Running-in
Wear
Bearings
Slip
Plastic deformation
Plastic flow

ABSTRACT

Running-in occurs in rolling-sliding contacts under mixed-friction conditions and typically involves asperity smoothing through mild wear and plastic deformation. To improve the prediction of service life or friction of rolling-element bearings under mixed-friction conditions, knowledge of surface topography changes during running-in and their dependence on the operating condition is an important prerequisite. Therefore, this study aims to describe the surface mechanisms due to wear, during running-in and their dependence on one of the variables, slip.

AISI 52100 steel specimens were tested in a mini traction machine (MTM) instrumented with friction and contact potential measurement in the presence of a PAO base oil, operating in the mixed lubrication regime. A novel method of pre and post-test surface relocation with 3-D optical profilometry and scanning electron microscopy (SEM) was implemented. Rolling-sliding tests were performed to study the effect of slide-roll ratio on the surface topography changes during running-in. Additional tests were conducted to track the changes to surface topography during this period.

The results exhibit the rapid nature of running-in and how most of the surface topography changes occur in the first few load cycles. Surface topography transitions such as asperity removal due to wear, increase in the load-bearing area of the asperities and in tests with slip, plastic flow of material from peaks into adjacent valleys are shown at high magnification. Surface profilometry measurements show that the reduction in depth of the valleys due to plastic flow adds to the reduction in roughness, thus accurately identifying the surface mechanism, and redressing the consensus that the reduction in roughness during running-in is mainly due to wear and plastic deformation diminishing the height of the peaks, which is true for ideal running-in alone.

1. Introduction

Rolling bearings are critical to the functioning of most machinery. They facilitate low-friction relative motion between machine elements while simultaneously transmitting the forces between them as well as guiding and positioning them relative to each other [1]. Though bearings can be used to enable a wide range of relative motions, they are commonly used to effectively reduce friction and support shafts of rotating machinery. They do so by employing subcomponents that rotate and slide.

Modern machinery with the aim of improving efficiency has led to higher power density and lower viscosity oils, both of which have pushed the lambda ratio (λ) lower, the formulation of which is shown below. It is computed using the ratio between the minimum film thickness, $h_{\min}$ and composite surface roughness, which is derived from the root mean square (RMS) roughness, R_q of the two surfaces in contact. The lowering of the lambda ratio (λ) in bearings influences the full film hydrodynamic lubrication towards mixed and boundary, which is accompanied by increased asperity-asperity interactions.

$$\lambda = \frac{h_{min}}{\sqrt{\left(R_{q1}^2 + R_{q2}^2\right)}}$$

Fig. 1 is the classic 'bath-tub curve' showing an idealised plot of wear and wear rate over time. Though not completely appropriate to bearing surfaces operating in ideal conditions, that tend to experience little to no wear due to their low roughness and typically fatigue fail due to stress concentration from the removal of roller profile, this 'bath-tub' curve

* Corresponding author.
E-mail address: msds1v16@soton.ac.uk (M.S.D. Sakhamuri).

https://doi.org/10.1016/j.wear.2023.204685
Received 19 September 2022; Received in revised form 17 December 2022; Accepted 29 December 2022
Available online 9 March 2023

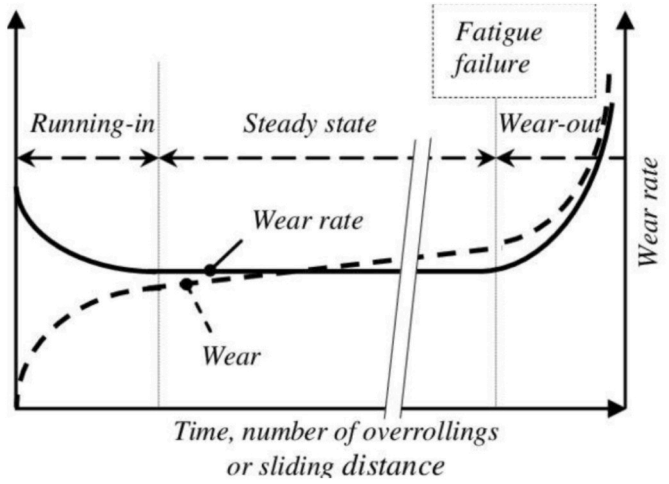

Fig. 1. Idealised wear and wear rate vs time [4].

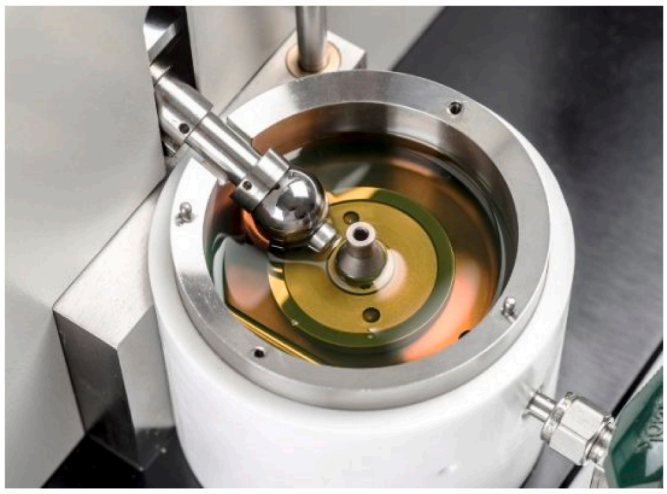

Fig. 2. Mini traction machine by PCS instruments [9].

provides a general understanding of wear and surface interaction during the running-in period before achieving steady state. The rate of wear is expected to be initially higher when the surfaces in contact are fresh and not perfectly conformal. This non-conformality leads to high local pressures, causing elastic deformation, plastic deformation and wear of the surface asperities [2,3]. This period is known as running-in, and the wear generated during this period is known as running-in wear.

As running-in progresses, asperities become more conformal, thus reducing the overall roughness of the surfaces. This allows for the lubricant to form a film and separate the surfaces from interacting with one another, thus pushing the lambda ratio (λ) higher and the lubrication regime from boundary/mixed to closer to full hydrodynamic lubrication. The wear rate is reduced due to reduced interaction between the surface asperities, and the bearing enters steady state operation. Ideal running-in is short and mild, and conditions the bearing surface to achieve its designed life [3].

However, there are instances where running-in can detriment the life of a bearing. Lower lubrication regime and high local pressures severely strain the surface to result in improper running-in where surface asperities experience excessive plastic deformation. It has also been indicated in prior research that pits appeared during the later stages of bearing operation at sites of extreme plastic deformation and high local pressures caused due to excessive running-in Ref. [2]. This way, the period of running-in affects the overall life of a bearing, and not just the steady state period of a bearing. Therefore, it is of importance to examine and understand the micro-level surface topography changes occurring during running-in.

Running-in research has been underway since 1933 when Abbott and Firestone [5] first showed that the rate of wear diminishes as peaks progressively become blunted [3]. The introduction of electrical contact resistance (ECR) in lubricated contacts has also helped further understand the asperity level changes at play during running-in. However, the understanding is not complete due to it being a derived parameter. Recent running-in research by Clarke et al. [2] went one step further by comparing individual asperities, pre and post running-in, using an in-situ 2-D profilometer. They showed, using 2-D profile traces, plastic deformation and wear of surface asperities. Hansen et al. [3] built on this existing research to show 3-D profilometry scans of surfaces before and after running-in. They concluded that running-in does not affect the valleys and this phenomenon results in unrealistic estimation of lubrication regime due to the lambda ratio (λ) calculation that factors in RMS roughness, R_q [3,6].

Most of these conclusions are true for ideal running-in, which is mild and affects the asperity peaks alone. This research examines surfaces that underwent running-in differently in a mini traction machine (MTM). This was achieved by running tests by incorporating slip at different slide-roll ratios (SRR), as slip is known to increase plastic deformation and the risk of pitting [7,8]. A novel technique is used to compare individual asperities of the MTM discs before and after running-in at the micro-level using relocation with a scanning electron microscope (SEM). In addition to comparing the disc surfaces qualitatively, the surfaces are compared quantitatively using areal roughness measurements from relocated 3-D profilometry scans. The areal roughness parameters are derived from a larger number of surface data points and provide a more accurate quantification of a surface when compared to 2-D profilometry scans and 2-D roughness measurements. The research is further supported by friction and ECR results from the MTM tests.

2. Experimental setup and methodology

2.1. Rig

The tests were conducted on a ball on disc tribometer. The tribometer is manufactured by PCS Instruments in London, United Kingdom and is called the Mini Traction Machine (MTM). Fig. 2 shows the MTM's ball and the disc in the main capsule, submersed in oil. The ball and the disc are independently driven and can achieve entrainment velocities in the range of −4 m/s to 4 m/s, while applying a load of up to 75 N, which translates to 1.25 G Pa for the samples used in this research.

2.2. Samples and lubricant

The AISI 52100 balls and discs used for the testing were manufactured and supplied by PCS Instruments. The balls and the discs were lapped in the final manufacturing process to achieve the required surface finish of R_q 0.02 μm and R_q 0.07 μm, respectively. The surface finish of the samples was specifically chosen to mimic bearing surfaces, which are sequentially ground and honed to achieve a surface finish of R_a 0.05

Table 1
Dimensions and material properties of the samples.

Material		Ball		Disc
		AISI 52100 Steel		
Radius in X Direction	R_{1x} **(mm)**	8.675	R_{2x} **(mm)**	0
Radius in Y Direction	R_{1y} **(mm)**	9.525	R_{2y} **(mm)**	0
Young's Modulus	E_1 **(GPa)**	207	E_2 **(GPa)**	207
Poisson's Ratio	V_1	0.29	V_2	0.29
RMS Roughness	R_{q1} **(μm)**	~0.02	R_{q2} **(μm)**	~0.07
Hardness	H_1 **(Hv)**	800	H_2 **(Hv)**	760

Table 2
Sensing and measurement techniques.

Measurement	Technique	Sampling Frequency
Load	Online	1 Hz
Speed of Samples	Online	1 Hz
Lubricant Oil Temperature	Online	1 Hz
Friction	Online	1 Hz
Contact Potential with a 10 kΩ balance resistor	Online	1 Hz
Surface Imaging, Roughness Measurement using 3-D Profilometry	Offline	Pre and Post Test using relocation
Surface Imaging using SEM	Offline	Pre and Post Test using relocation

Table 3
Phase 1: Tests studying the influence of slip, on running-in.

Test Name	Common Test Variables	Slide-Roll Ratio	Duration
Test 1	**Maximum Pressure:** 1 GPa **Load:** 37 N	0	179 min/300k cycles
Test 2	**Entrainment Velocity:** 3.7 m/s **Oil:** PAO base oil at 100 °C	0.06	174 min/300k cycles
Test 3	**Roughness (R_q):** 0.02 μm (ball) vs 0.07 μm (disc) **Lambda Ratio (λ):** 1.15	0.12	169 min/300k cycles

μm [10]. The smooth finish and the curvature of the balls does not allow for accurate profile measurements and surface imaging, and therefore are not discussed in this research. However, the influence of the ball on the film forming capability of the contact is insignificant due to the relatively much lower roughness of the ball when compared to the disc.

A summary of the dimensions and the material properties of the samples is shown in Table 1. The difference between the contact radius in the X direction (circumferential) and contact radius in the Y direction (axial) of the ball is due to its axis of rotation being 24.4° angle from the surface of the disc.

The samples are tested in a Polyalphaolefin (PAO) synthetic base oil at 100 °C. The dynamic viscosity of the oil at 100 °C is 0.005393 Pa s. The contact, as shown in Fig. 2, is submersed in oil to avoid adhesive wear and material transfer, which tend to occur in bearing surfaces suffering from inadequate lubrication [11,12].

2.3. Sensing and measurement

The sensing and measurement techniques used for the ball on disc tribometer tests are summarised in Table 2.

The online techniques shown in Table 2 are in-built into the MTM software and acquired at a constant sampling frequency of 1 Hz.

The surface imaging and roughness measurement were conducted using the Alicona G4 InfiniteFocus with an error margin of 2 nm. The equipment is manufactured by Bruker Alicona in Austria and uses an image-based Z (vertical) direction stacking system to compute heights. Two points on the wear patch were relocated using micro-hardness indents outside the wear patch and measured.

The surface of the discs was also examined under a SEM. The micro-hardness indents allowed for relocation of individual asperities at high magnification. Pre and post-test comparison of these asperities is discussed in the subsequent sections.

2.4. Tests

The testing is split into two phases. The first phase is summarised in Table 3. This testing phase aims to investigate the effect of slip on running-in and differentiate between the different types of running-in. The maximum pressure, load, entrainment velocity and oil temperature were adjusted to achieve a lambda ratio (λ) of 1.15, which is categorised as the lower end of mixed lubrication regime and the operating region for roller element bearings. SRR was varied between 0 and 0.12 in the three tests as this represents the operating range for most roller element bearings. The duration of the tests was adjusted to ensure the discs in the three tests undergo 300k cycles respectively. It is known, from research finding of Clark et al. [2] that majority of the roughness changes and asperity deformation occurs during the initial contact cycles, less than 1000 cycles. The 300k cycles test duration allows for the investigation of the surface changes due to running-in and provides an understanding of the surface in the steady state phase.

Table 4
Phase 2: Interval tests tracking surface changes during running-in.

Test Name	Common Test Variables	Duration
Interval Test 1	**Maximum Pressure:** 1 GPa **Load:** 37 N	1 s/28 cycles
Interval Test 2	**Entrainment Velocity:** 3.7 m/s **SRR:** 0.06	1 s/28 cycles
Interval Test 3	**Oil:** PAO base oil at 100 °C **Roughness (R_q):** 0.02 μm (ball) vs 0.07 μm (disc) **Lambda Ratio (λ):** 1.15	58 s/1624 cycles

The second phase of testing tracked some of the surface phenomenon seen in the first part of testing by running interval tests on one set of ball and disc and conducting the surface measurements discussed in section 2.3 during the intervals. These tests are summarised in Table 4.

3. Results and discussion: phase 1

This section of the paper details and discusses the results from Phase 1. These tests study the influence of induced slip on running-in and Table 3 summarises the tests conducted in this phase.

3.1. Optical profilometry

Figs. 3–5 show the optical profilometry images of the pre-tested and post-tested discs from Test 1, Test 2 and Test 3. As evident from the heat map, the surfaces underwent running-in. Locations A, B and C in Fig. 3 and Locations A and B in Figs. 4 and 5 show diminished heights of asperities after testing.

In addition to the wear of the asperity peaks, instances of plastic deformation are shown at sites D and E in Fig. 3 (0 SRR) and at sites D, E and F in Fig. 4 (0.06 SRR) and Fig. 5 (0.12 SRR). The amount of plastic deformation is minimal in Test 1 (0 SRR). However, in Test 2 (0.06 SRR) and Test 3 (0.12 SRR), significant plastic deformation is seen from the optical profilometry heat maps turning greener after testing. There also appears to be a heavy amount of plastic flow of material into the valleys.

This amount of plastic deformation and material flow, in tests with induced slip, is detrimental to the life of the contact and is shown to cause pitting, especially when exposed to oils with anti-wear additives like Zinc Dialkyl Dithio Phosphates (ZDDP) [2,7,13].

The optical profilometry results have shown a difference between surface changes caused due to induced slip. However, these results cannot be used as conclusive proof for the observed asperity level changes. This is due to the zero-level adjustment required with profilometry in general. To compare two sets of profilometry data, a zero-level must be established. In running-in research, this is established by matching the depth of the valleys based on the assumption that running-in is a top-level asperity phenomenon and does not affect the valleys. However, this cannot be assumed for instances where running-in involves plastic deformation and flow of material into the valleys. Therefore, a conclusive approach in the form of SEM was used to support the surface phenomenon seen in the optical profilometry images.

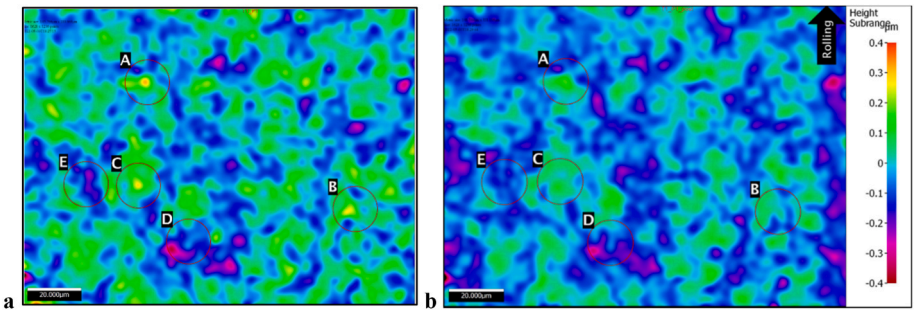

Fig. 3. Optical Profilometry of the disc a) before and b) after Test 1 (0 SRR).

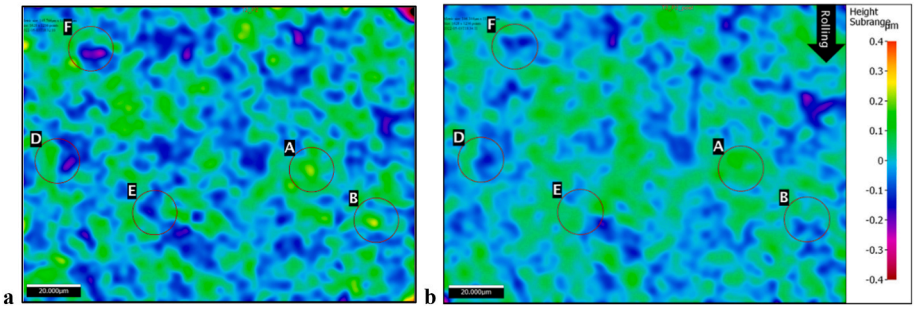

Fig. 4. Optical Profilometry of the disc a) before and b) after Test 2 (0.06 SRR).

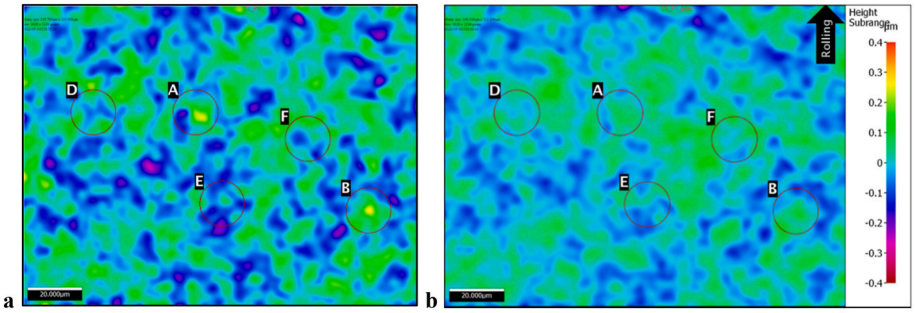

Fig. 5. Optical Profilometry of the disc a) before and b) after Test 2 (0.12 SRR).

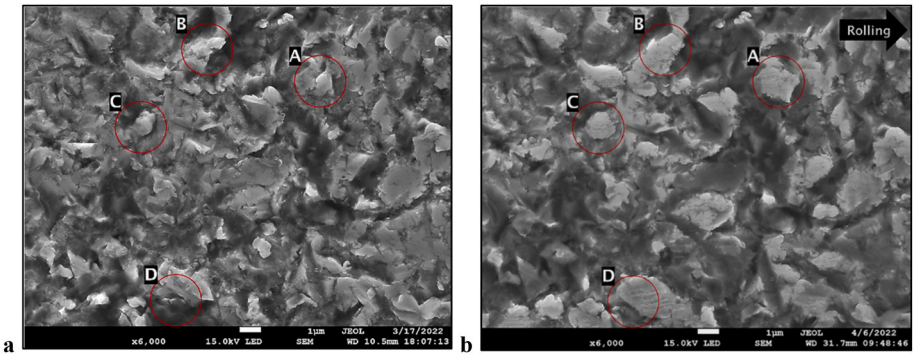

Fig. 6. SEM of the disc a) before and b) after Test 1 (0 SRR).

3.2. Scanning electron microscopy (SEM)

Figs. 6–8 show the SEM scans of the pre-tested and post-tested contact patch of the discs from Test 1 (0 SRR), Test 2 (0.06 SRR) and Test 3 (0.12 SRR). These areas were meticulously relocated to scan at 6000x and identify plastic deformation to individual asperities in the contact patch.

As seen previously in the optical profilometry images, the disc from Test 1 (0 SRR), did not undergo significant plastic deformation. A few instances of plastic deformation can be seen at sites A, B, C and D, where asperities have plastically deformed due to contact pressure and the load bearing area of the contact was maximised. However, in this instance,

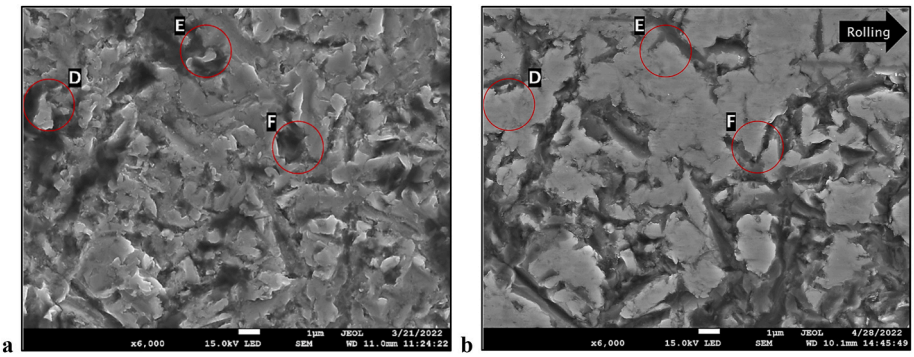

Fig. 7. SEM of the disc a) before and b) after Test 2 (0.06 SRR).

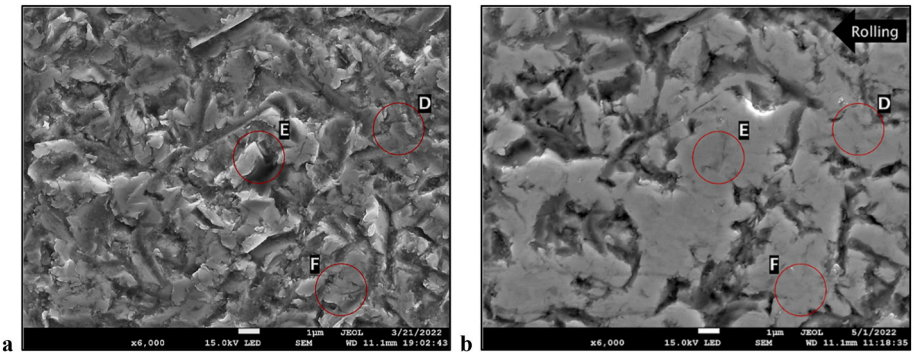

Fig. 8. SEM of the disc a) before and b) after Test 3 (0.12 SRR).

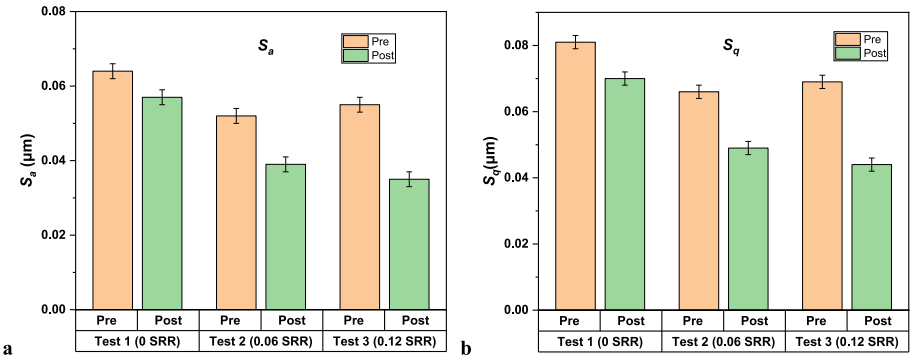

Fig. 9. a) S_a and b) S_q of the pre-tested and post-tested discs.

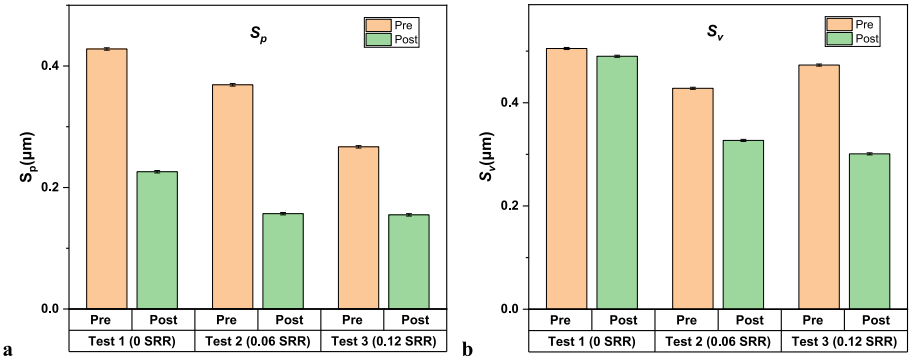

Fig. 10. a) S_p and b) S_v of the pre-tested and post-tested discs.

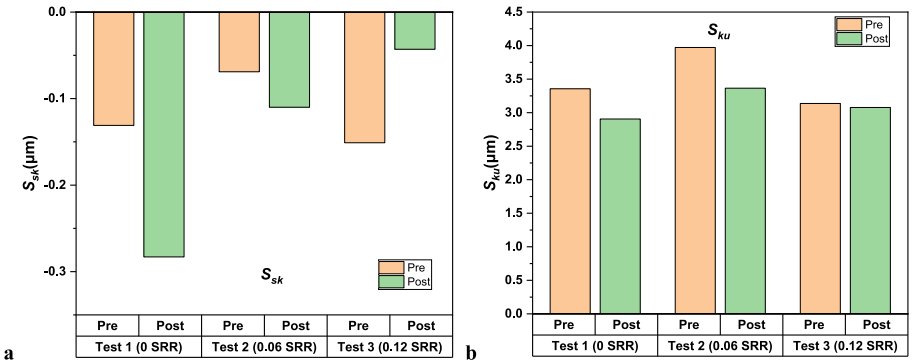

Fig. 11. a) S_{sk} and b) S_{ku} of the pre-tested and post-tested discs.

the valleys in the contact are mostly unchanged.

The scans of the discs from Test 2 (0.06 SRR) and Test 3 (0.12 SRR) reiterate the significant amount of plastic deformation previously seen from the optical profilometry images. Plastic deformation and material flow from asperity peaks into adjacent valleys is evident from sites D, E and F in Fig. 7 (0.06 SRR) and Fig. 8 (0.12 SRR). The scans also provide a reasoning to the reduction in surface roughness during the running-in period, which is evidenced to have been caused by the change in both the asperity peaks and valleys. Due to this, the reduction in roughness is complimented by normalisation of the surface.

3.3. Roughness

The relocated optical profilometry scans from section 3.1 were filtered using a 0.25 mm Gaussian filter and used to compute the surface texture parameters (height).

Fig. 9 shows the average roughness S_a and the RMS roughness S_q of the pre-tested and post-tested samples from Test 1 (0 SRR), Test 2 (0.06 SRR) and Test 3 (0.12 SRR). The data shows a consistent reduction in both S_a and S_q for all the tested discs. The reduction is the largest for the disc that underwent 0.12 SRR, followed by 0.06 SRR and 0 SRR. This can be pinpointed to surface changes seen from the SEM scans in section 3.2 and can be attributed to excessive plastic deformation affecting the valleys, in addition to the peaks in tests with induced slip.

Fig. 10 shows the maximum peak height (S_p) and maximum valley depth (S_v) of the pre-tested and post-tested samples from Test 1 (0 SRR), Test 2 (0.06 SRR) and Test 3 (0.12 SRR). A consistent decrease in the S_p values is evident from the data with the post-test S_p values being lower for the tested discs with induced slip.

The S_v values for Test 1 (0 SRR) has remained unchanged despite testing. This is evidence of minimal plastic deformation and material flow from peaks into the adjacent valleys, as previously seen in the SEM scans. The tests with induced slip, Test 2 (0.06 SRR) and Test 3 (0.12 SRR) show decreased S_v values after testing, with the 0.12 SRR test showing a larger decrease when compared to the 0.06 SRR. This is attributed to the increased plastic deformation from the additional slip, which is evident from the SEM scans in the previous section.

Fig. 11 shows the skewness (S_{sk}) and kurtosis (S_{ku}) of the pre-tested and post-tested samples from Test 1 (0 SRR), Test 2 (0.06 SRR) and Test 3 (0.12 SRR). The tested disc from Test 1 (0 SRR) shows a decreased S_{sk} value due to the majority of the surface transformations resulting from wear of the asperity peaks. The decline in S_{sk} value for Test 2 (0.06 SRR) is minimal compared to Test 1 (0 SRR) due to the decrease in valley depth from plastic deformation and material flow contradicting the decrease in asperity heights. However, the tested disc from Test 3 (0.12 SRR) shows an increase in S_{sk} value, thus quantitatively showing the significantly more decrease in valley depth when compared to the decrease in height of the asperity peaks.

S_{ku} of the tested samples from all the tests reduced towards 3, which is a characteristic of a normal distribution. The surface asperities of the

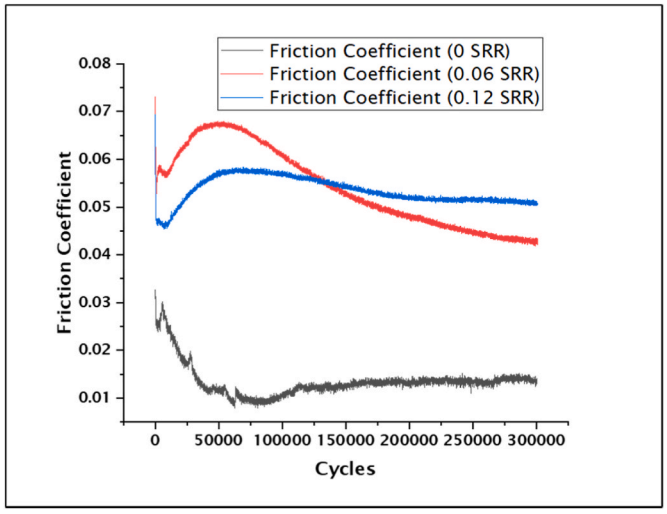

Fig. 12. Friction vs cycles during Test 1 (0 SRR), Test 2 (0.06 SRR) and Test 3 (0.12 SRR).

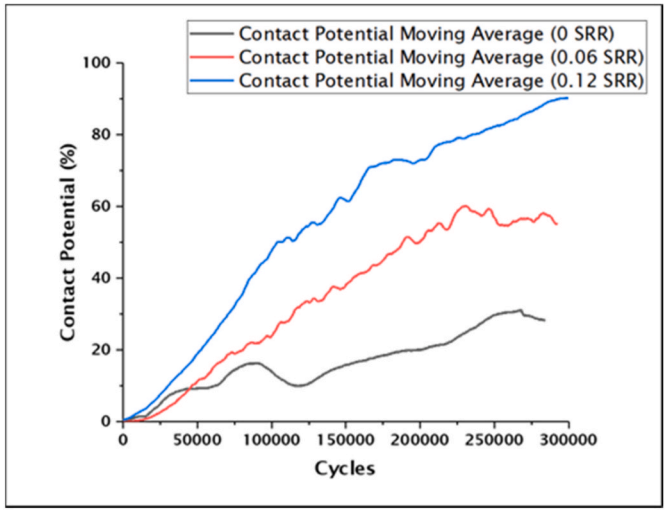

Fig. 13. Contact Potential vs cycles during Test 1 (0 SRR), Test 2 (0.06 SRR) and Test 3 (0.12 SRR).

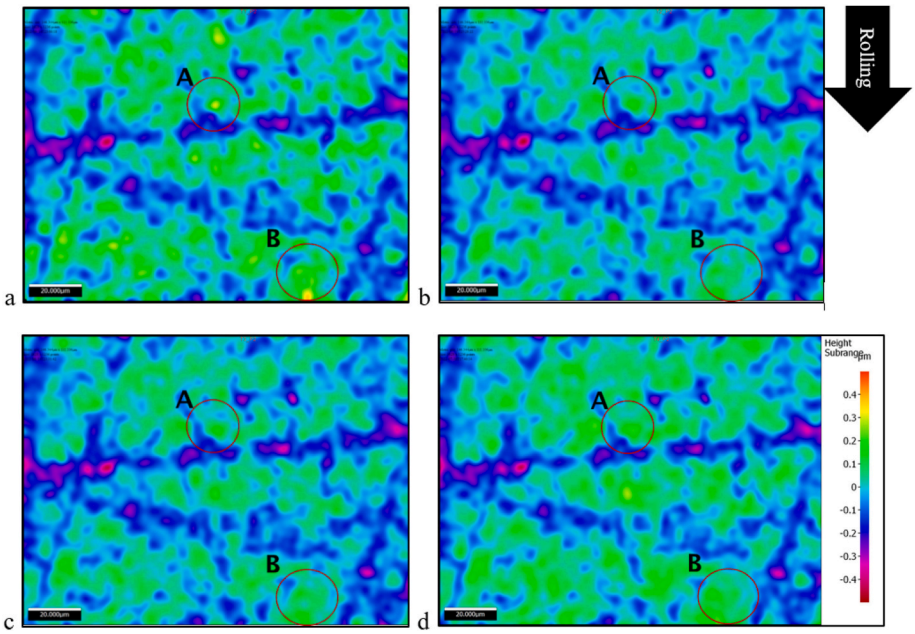

Fig. 14. Optical profilometry of the disc at a) 0 cycles, b) 28 cycles, c) 56 cycles and d) 1680 cycles.

samples underwent normalisation due to running-in which was evident from the SEM scans in the previous section.

3.4. Friction and contact potential

Fig. 12 shows the plotted friction data acquired during the three tests. The friction undergoes a drop during the initial cycles for all the tests. The drop is instantaneous in the case of the rolling-sliding tests, Test 2 (0.06 SRR) and Test 3 (0.12 SRR), when compared to Test 1 (0 SRR), the pure rolling test. This drop is due to the highest asperity peaks undergoing wear and plastic deformation during the initial cycles. These asperity peaks experienced wear and plastic deformation at a much higher rate in Test 2 (0.06 SRR) and Test 3 (0.12 SRR) due to the higher relative velocity between the contacting surfaces from the induced slip. The friction during Test 1 (0 SRR), the pure rolling tests, is significantly lower when compared to rolling-sliding contacts. This phenomenon of rolling contacts experiencing less friction when compared to sliding contacts is well known and has been documented in research by Zhang et al. [14], Ciulli et al. [15] and Hansen et al. [6]. Section 4.4 discusses the other trends in friction data in detail after evidence from testing in Phase 2.

The contact potential data plotted from Fig. 13 shows an increasing

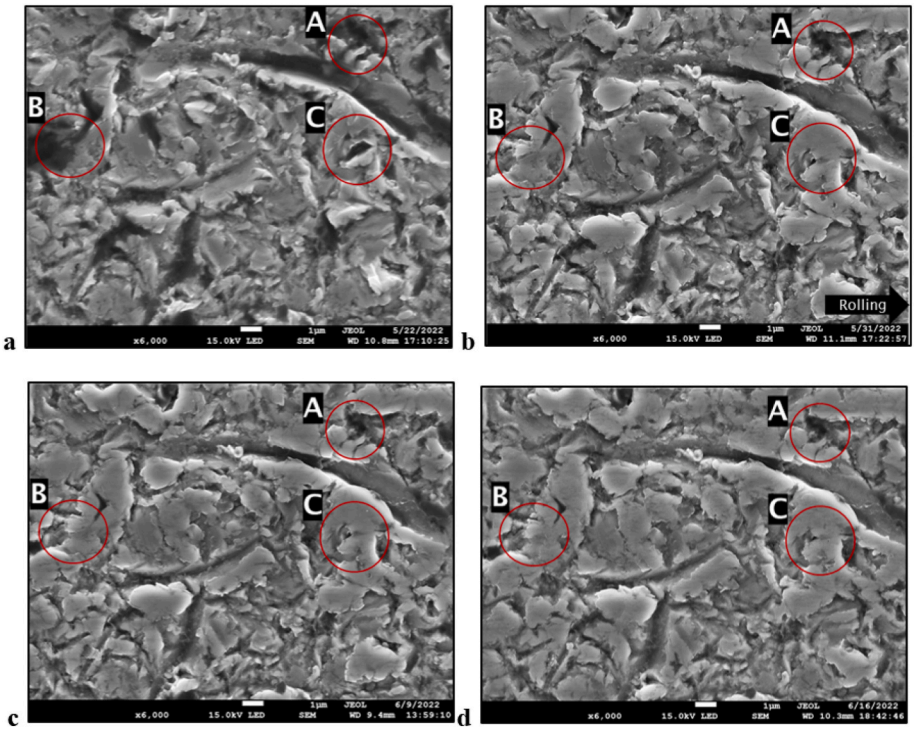

Fig. 15. SEM of the disc at a) 0 cycles, b) 28 cycles, c) 56 cycles and d) 1680 cycles.

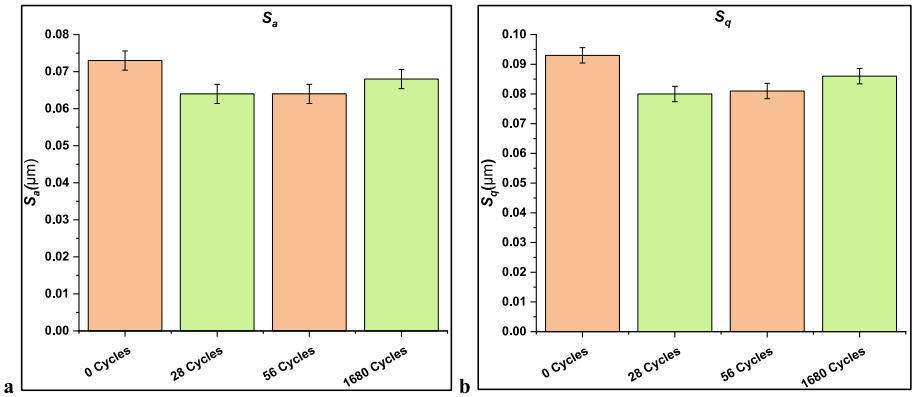

Fig. 16. a) S_a and b) S_q of the disc at 0 cycles, 28 cycles, 56 cycles and 1680 cycles.

electrical resistance in the contact from the non-polar nature of the base oil through the duration of all the tests. However, the data is skewed due to a small percentage of contacting asperities heavily influencing the electrical resistance of the contact. Though contact potential measurement can be an excellent method to identify the lubrication regime in the contact, it is not linearly influenced by surface topography changes. This is demonstrated in the next section where interval testing is conducted to show that the majority of the roughness reduction during running-in occurs in the initial few cycles which is contrary to the steady rise in contact potential.

3.5. Discussion

The significant plastic deformation seen between the pure rolling test, Test 1 (0 SRR) and the tests with induced slip, Test 2 (0.06 SRR) and Test 3 (0.12 SRR) is due to a multitude of reasons. Firstly, the addition of slip causes a lower than assumed lubricant film and lambda ratio (λ). The Dowson and Higginson [16] elasto-hydrodynamic model used for the calculation of lambda ratio (λ) does not account for changes in slip. This is contrary to optical interferometry testing that showed reduction in the central film thickness with the addition of slip [8]. This results in an increase in the amount of asperity deformation required to achieve full film lubrication. However, the effect of the range of SRR used in this testing on the lubricant film thickness is minimal based on research conducted by Yagi et al. [8]. Secondly, an increase in slip increases the micro-contact stress cycles, thus causing more wear and plastic deformation to the surface asperities [7]. And lastly, an increase in slip results in an increase in friction as seen in Fig. 12. As the friction coefficient increases the initial plastic zone moves closer to the surface and unconstrained plastic flow occurs at a lower normal pressure [17]. Since the normal pressure is kept constant between the three tests, the tests with induced slip experienced significantly more plastic deformation and material flow. This is shown to increase the risk of pitting, especially when exposed to oils with anti-wear additives, like ZDDP, due to cyclic loads and concentration of stresses in the sub-surface region [2,7,13].

4. Results and discussion: phase 2

This section details and discusses the results from the second phase of testing. Interval tests were conducted to track and investigate the surface topography changes during the initial contact cycles. The tests were conducted at 0.06 SRR until 1680 cycles and are summarised in Table 4.

4.1. Optical profilometry

Fig. 14 shows the optical profilometry scans of the disc at 0, 28, 56 and 1680 cycles. Sites A and B in Fig. 14 show areas of the contact patch where asperity peaks underwent wear. However, the optical profilometry scans do not show any evidence of significant plastic deformation at this early stage.

4.2. Scanning Electron Microscopy (SEM)

Fig. 15 shows the surface topography of the disc at 0, 28, 58 and 1680 cycles using a SEM. The SEM images, unlike the optical profilometry scans, show some amounts of plastic deformation at sites A, B and C. Based on SEM scans of the discs from Test 2 (0.06 SRR) in Phase 1 testing, the changes to the surface topography are not complete. The surface is yet to undergo significant amounts of plastic deformation. However, this testing proves that the top-level asperity wear occurs in the initial contact cycles, in this case less than 28 cycles (sliding distance = 0.23 m) and is followed by gradual plastic deformation and flow. This

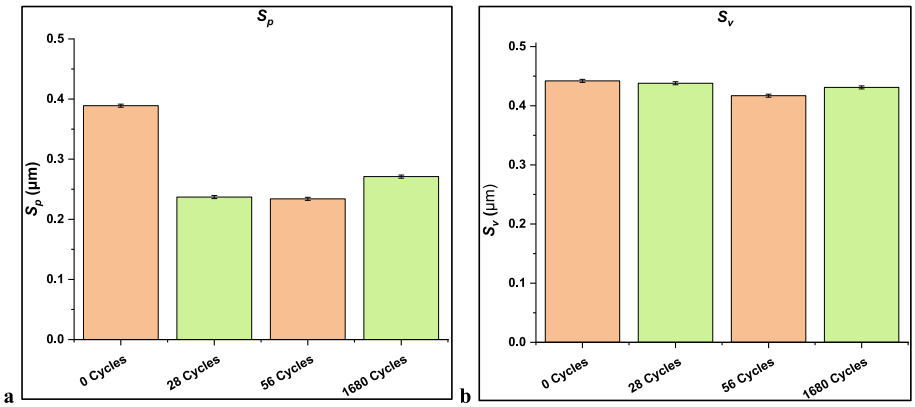

Fig. 17. a) S_p and b) S_v of the disc at 0 cycles, 28 cycles, 56 cycles and 1680 cycles.

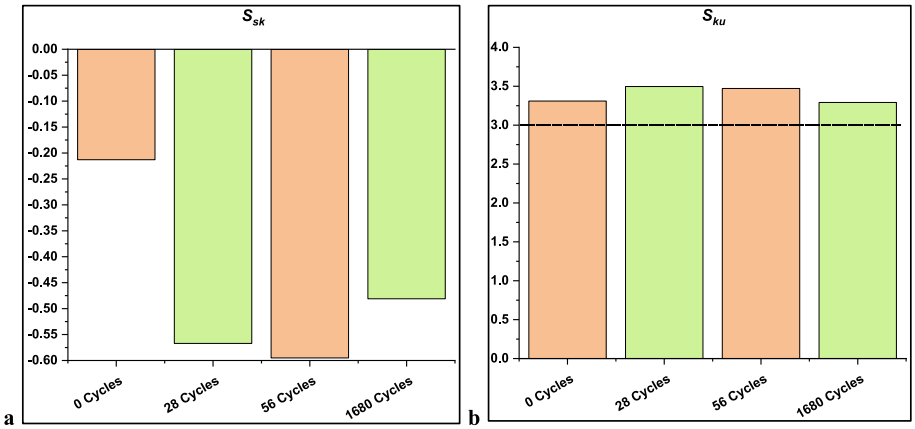

Fig. 18. a) S_{sk} and b) S_{ku} of the disc at 0 cycles, 28 cycles, 56 cycles and 1680 cycles.

is further supported with the roughness results in the next section.

4.3. Roughness

Fig. 16 shows the S_a and S_q measurements of the optical profilometry scans at 0, 28, 56 and 1680 cycles. The S_a and S_q drop sharply after 28 cycles (sliding distance = 3.7 m) due to wear and plastic deformation of the asperity peaks. This is evident from the S_p values in Fig. 17, which show a sharp drop in the maximum peak height, per cut-off area. However, the S_a, S_q and S_p increase in value after 1680 cycles (sliding distance = 13.3 m). This is discussed in section 4.4.

S_{sk} and S_{ku} values are shown in Fig. 18. S_{sk} undergoes a significant drop after 28 cycles due to wear and plastic deformation of the asperity peaks and skewing the surface more towards the negative side. S_{sk} increases at 1680 cycles (sliding distance = 3.7 m) due to the increase in the S_p value.

S_{ku} values can be unpredictable during these initial contact cycles, where a combination of surface changes can occur. However, in the later stages, the S_{ku} value will move towards 3 when the surface becomes normally distributed, as previously seen in section 3.3.

4.4. Discussion

Based on the two phases of testing and friction data from Phase 1, step wise surface topography changes occurring during running-in can be listed.

- The fresh surfaces undergo wear of the asperity peaks during the initial contact cycles. This is evident from the optical profilometry scan of the disc operated under 0.06 SRR in Phase 2 after 28 cycles. This is supported by research conducted by Clarke et al. [2].
- In the case of ideal running-in, the surface roughness reduces and pushes the contact from mixed to micro elastohydrodynamic lubrication (EHL) [3]. The bearing surfaces are completely separated by a lubricant film at this stage and the bearing is said to enter steady state.
- In other cases of running-in, the surfaces are still in contact despite the preliminary reduction in roughness. The blunted surface asperities undergo a complex cycle of formation due to compressive stresses, plastic deformation due to shearing and wear due to separation [17]. This is evident from the friction data in Phase 1, where an increase in friction is seen after the initial drop in Test 2 (0.06 SRR) and Test 3 (0.12 SRR) due to this cycle of asperity formation, shearing and separation in blunt asperities. Further evidence of formation is detected from the increase of S_a, S_q and S_p in Phase 2 after 1680 cycles (sliding distance = 13.3 m).
- This stage is ended when the surface roughness drops significantly to push the system into micro-EHL, However, in cases of extremely thin oil films, surface contact might persist and result in a deeper contact patch and more plastic deformation as evidenced in tests conducted in boundary lubrication in previous research [13].
- This results in surfaces completely normalising from the asperity peak removal due to wear and asperity valley filling from material flow.

5. Conclusion

The two phases of experimental tests and measurements resulted in new findings about surface topography changes during running-in in rolling-sliding contacts. Previous research considered running-in as mild wear affecting the asperity peaks. However, from this research, it is evident that running-in can take different forms.

Running-in conditions the surface through mild wear and prevents cyclic loading of the sub surface and pitting, thus ensuring maximum intended life of a bearing surface [2]. An example of this running-in was show in Test 1 (0 SRR) in Phase 1 of testing.

However, when surfaces are run in low lambda ratios and high amounts of slip (λ), in addition to wear of the asperity peaks, significant plastic deformation and material flow occurs, thus causing increased sub-surface stresses that might result in pitting [2]. Evidence of this form of running-in was seen in the tests conducted with induced slip.

Though, there is partial evidence that plastic deformation during the running-in stage promotes early onset of pitting due to cyclic loading after the formation of a lubricant film, sub surface evidence of this mechanism is yet to be identified. Therefore, future research to investigate precursors to pitting that arise from significant plastic deformation is envisaged.

Declaration of competing interest

The authors declare that they have no known competing financial interests or personal relationships that could have appeared to influence the work reported in this paper.

References

[1] C. Brecher, CIRP Encyclopedia of Production Engineering, Springer International Publishing, 2014, 80-80.
[2] A. Clarke, I.J.J. Weeks, R.W. Snidle, H.P. Evans, Running-in and micropitting behaviour of steel surfaces under mixed lubrication conditions, Tribol. Int. 101 (2016) 59–68, https://doi.org/10.1016/j.triboint.2016.03.007.
[3] J. Hansen, M. Björling, R. Larsson, Topography transformations due to running-in of rolling-sliding non-conformal contacts, Tribol. Int. 144 (2020), https://doi.org/10.1016/j.triboint.2019.106126.
[4] Jamari, Running-in as an engineering optimization, J Ti Undip Jurnal Teknik Industri 2 (1) (2007) 1–10, https://doi.org/10.12777/jati.2.1.1-10.

[5] E. J. Abbott and F. A. Firestone, "Specifying Surface Quality: a method based on accurate measurement and comparison," J. Mech. Eng. 55, 1933..
[6] J. Hansen, Elasto-hydrodynamic Film Formation in Heavily Loaded Rolling-Sliding Contacts, Doctor of Philosophy, Engineering Sciences and Mathematics, Lulea University of Technology, Lulea, 2021.
[7] P. Rycerz, A. Kadiric, The influence of slide–roll ratio on the extent of micropitting damage in rolling–sliding contacts pertinent to gear applications, Tribol. Lett. 67 (2) (2019) 63, https://doi.org/10.1007/s11249-019-1174-7, 2019/05/11.
[8] K. Yagi, K. Kyogoku, T. Nakahara, Experimental investigation of effects of slip ratio on elastohydrodynamic lubrication film related to temperature distribution in oil films, Proc. IME J. J. Eng. Tribol. 220 (4) (2006) 353–363, https://doi.org/10.1243/13506501JET154, 2006/04/01.
[9] PCSInstruments. "MTM." https://pcs-instruments.com/product/mtm/(accessed 3/January/2022..
[10] N. Jouini, P. Revel, G. Thoquenne, Investigation of surface integrity induced by various finishing processes of AISI 52100 bearing rings, Materials 15 (10) (May 22 2022), https://doi.org/10.3390/ma15103710.
[11] M. Fowell, S. Ioannides, A. Kadiric, An experimental investigation into the onset of smearing damage in nonconformal contacts with application to roller bearings, Tribol. Trans. 57 (3) (2014) 472–488, https://doi.org/10.1080/10402004.2013.875607.
[12] F.D. Rowe, Diagnosis of rolling contact bearing damage, 1971, pp. 137–146, https://doi.org/10.1016/0041-2678(71)90025-X, vol. 4, no. 3.
[13] M. Ueda, H. Spikes, A. Kadiric, In-situ observations of the effect of the ZDDP tribofilm growth on micropitting, Tribol. Int. 138 (2019) 342–352, https://doi.org/10.1016/j.triboint.2019.06.007.
[14] X. Zhang, S. Kanapathipillai, T. Wu, Z. Peng, Frictional behaviour and friction mechanisms of rolling-sliding contact in mixed EHL, Tribol. Int. 114 (2017), https://doi.org/10.1016/j.triboint.2017.04.032, 04/01.
[15] E. Ciulli, K. Stadler, T. Draexl, The influence of the slide-to-roll ratio on the friction coefficient and film thickness of EHD point contacts under steady state and transient conditions, Tribol. Int. 42 (4) (2009) 526–534, https://doi.org/10.1016/j.triboint.2008.04.005, 2009/04/01/.
[16] Dowson, D, A central film thickness formula for elastohydrodynamic line contacts, elastohydrodynamics and related topics, 60, in: Proc. 5th Leeds-Lyon Symp, 1978 [Online]. Available: http://ci.nii.ac.jp/naid/10012874308/en/.
[17] D. Arnell, Mechanisms and laws of friction and wear, in: Tribology and Dynamics of Engine and Powertrain, 2010, pp. 41–72.